Inorganic Chemistry

Article

pubs.acs.org/IC

Fabrication of $La_2Ti_2O_7$ Crystals Using an Alkali-Metal Molybdate Flux Growth Method and Their Nitridability To Form $LaTiO_2N$ Crystals under a High-Temperature NH_3 Atmosphere

Mirabbos Hojamberdiev,[†] Akiko Yamaguchi,[†] Kunio Yubuta,[‡] Shuji Oishi,[†] and Katsuya Teshima*[,†,§]

[†]Department of Environmental Science and Technology, Faculty of Engineering, and [§]Center for Energy and Environmental Science, Shinshu University, 4-17-1 Wakasato, Nagano 380-8553, Japan

[‡]Institute for Materials Research, Tohoku University, Sendai 980-8577, Japan

Supporting Information

ABSTRACT: Flux growth is a promising method that allows one to control over the crystalline phase, crystal shape, crystal size, and crystal surface through the selection of a suitable flux. In this work, lanthanum titanate ($La_2Ti_2O_7$) crystals with different morphologies were grown using the Na_2MoO_4, K_2MoO_4, NaCl, and mixed NaCl + K_2MoO_4 (molar ratio = 3:7) fluxes, and their nitridability to form $LaTiO_2N$ crystals under a high-temperature NH_3 atmosphere was also investigated. The effects of the solute concentration and cooling rate on the growth of the $La_2Ti_2O_7$ crystals were also studied. The X-ray diffraction results revealed that the {100} plane was dominant in the $La_2Ti_2O_7$ platelet crystals grown using the alkali-metal molybdate fluxes. When the solute concentration was increased from 1 to 20 mol %, the average size of the crystals decreased without considerable alteration of the overall crystal morphology. The $La_2Ti_2O_7$ crystals with the preferred ⟨010⟩ and ⟨001⟩ growth directions along the *b* and *c* axes were grown using the Na_2MoO_4 and K_2MoO_4 fluxes, respectively. Compared to the Na_2MoO_4 flux, the K_2MoO_4 flux did not show a cooling-rate-dependent effect on the growth of the $La_2Ti_2O_7$ crystals. It was found that conversion of the $La_2Ti_2O_7$ crystals to the $LaTiO_2N$ crystals was strongly dependent on the flux used to grow the precursor $La_2Ti_2O_7$ crystals. That is, the $La_2Ti_2O_7$ crystals grown using the K_2MoO_4 and NaCl fluxes were nearly completely converted into the $LaTiO_2N$ crystals, while conversion of the $La_2Ti_2O_7$ crystals grown using the Na_2MoO_4 and mixed NaCl + K_2MoO_4 fluxes to the $LaTiO_2N$ crystals seemed to be not completed yet even after nitridation at 950 °C for 15 h using NH_3 because of the larger crystal size and the presence of unintentional impurities (sodium and molybdenum from the flux) in the $La_2Ti_2O_7$ crystal lattice. Nevertheless, the $LaTiO_2N$ crystals fabricated by nitriding the $La_2Ti_2O_7$ crystals grown using the K_2MoO_4 and NaCl fluxes should be suitable for direct solar water splitting.

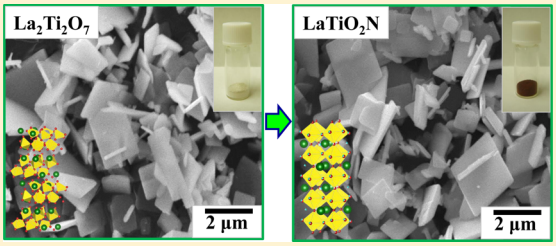

1. INTRODUCTION

Perovskite-type oxides and oxynitrides with favorable crystallographic flexibility allowing tuning of physical properties have been extensively studied for a wide range of applications. Lanthanum titanate ($La_2Ti_2O_7$) is a member of the perovskite layer structure family of ferroelectrics. The crystal structure of $La_2Ti_2O_7$ is built from the perovskite slabs stacked along the *a* axis, which are made up of corner-sharing TiO_6 octahedra and coordinated lanthanum cations. Each slab is four octahedra thick and is linked to a neighboring slab by lanthanum cations lying near the boundary,[1,2] as shown in Figure 1a. The $La_2Ti_2O_7$ compound crystallizes in a monoclinic perovskite-layered structure with the $P2_1$ space group. The lattice constants of monoclinic $La_2Ti_2O_7$ are a = 7.812(2) Å, b = 5.5440(7) Å, c = 13.010(2) Å, and β = 98.66°.[3,4] $La_2Ti_2O_7$ is characterized by its high Curie temperature (1773 K), spontaneous polarization (P_S = 5 μC cm^{-2}), and permittivity (ε = 42−62), making it a good candidate for high-temperature piezoelectric and ferroelectric random access memory and as a ferroelectric gate field-effect transistor, a high-temperature transducer, an electrooptic device, and a low-temperature coefficient of capacitance material.[5−11] Moreover, $La_2Ti_2O_7$ can also act as a host material for the substitution of La or Ti by

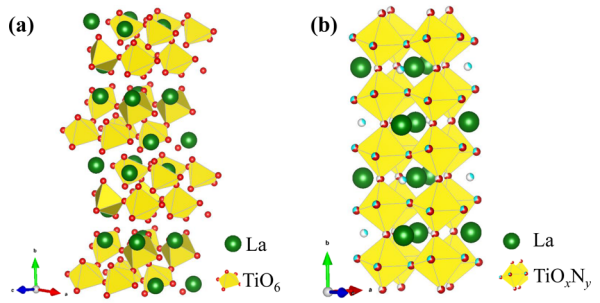

Figure 1. Schematic representation of the idealized crystal structures of (a) $La_2Ti_2O_7$ and (b) $LaTiO_2N$.

Received: November 30, 2014
Published: March 19, 2015

DOI: 10.1021/ic502862t
Inorg. Chem. 2015, 54, 3237−3244

Table 1. Experimental Conditions for the Flux Growth of $La_2Ti_2O_7$ Crystals

		solute		flux				
run	solute concn (mol %)	La_2O_3 (g)	TiO_2 (g)	$Na_2MoO_4{\cdot}2H_2O$ (g)	K_2MoO_4 (g)	NaCl (g)	holding temperature (°C)	cooling rate (°C h^{-1})
1	20	2.489	1.220	7.392			1100	50
2	10	0.697	0.341	4.655			1100	50
3	5	0.741	0.363	10.453			1100	50
4	1	0.156	0.077	11.476			1100	50
5	5	0.741	0.363	10.453			1100	5
6	5	0.741	0.363	10.453			1100	100
7	20	2.266	1.111		6.624		1100	50
8	10	1.239	0.608		8.153		1100	50
9	5	0.650	0.319		9.031		1100	50
10	1	0.135	0.066		9.798		1100	50
11	5	0.650	0.319		9.031		1100	5
12	5	0.650	0.319		9.031		1100	100
13	5	2.041	1.001			6.958	1000	50
14	5	0.817	0.401		7.946 (70%)	0.836 (30%)	1000	150

various lanthanide ions to produce phosphors emitting a wide variety of colors for the development of photoluminescent materials.[12] $La_2Ti_2O_7$ with a highly donor-doped layered perovskite structure has also demonstrated good photocatalytic activity for water splitting[13] and the decomposition of toxic organic substances.[14] According to Abe et al.,[15] an enhanced photocatalytic activity for water splitting of $La_2Ti_2O_7$ is closely related to the network of octahedral units of metal cations that increases the mobility of electrons and holes.

Lanthanum titanium oxynitride ($LaTiO_2N$) is a derivative of lanthanum(III) titanium(IV) oxide, in which oxygen is partially substituted by nitrogen under high-temperature nitridation using NH_3. Because oxygen is partially substituted by nitrogen, the N 2p levels are located above the O 2p levels, causing the reduction of a band gap.[16,17] As illustrated in Figure 1b, the $LaTiO_2N$ phase exhibits an orthorhombic structure with space group *Imma* and lattice constants of a = 5.5731(2) Å, b = 7.8708(3) Å, c = 5.6072(2) Å, and $\alpha = \beta = \gamma = 90°$. The tilt system of *Imma* $LaTiO_2N$ is $a^0b^-b^-$, and the antiphase tilt angle estimated is 10.404(5)°.[18] $LaTiO_2N$ is an n-type semiconductor with a perovskite-type structure and a band gap of 2.1 eV that shows good photocatalytic activity for H_2 and O_2 evolution from water splitting in the presence of suitable sacrificial reagents under irradiation of light with wavelengths up to ca. 600 nm due to its suitable band positions.[19,20] It has also been reported that the rate of O_2 evolution from $LaTiO_2N$ can be enhanced by loading with IrO_2,[19] CoO_x,[21] In_2O_3,[22] and Co_3O_4[23] as well as by a particle-transfer method,[24] the removal of defective surface reconstructed layers,[25] and $TiCl_4$ treatment.[26]

Furthermore, photocatalytic crystallites with clear crystal habits and high crystallinity can support a discrete loading of cocatalyst onto different surfaces. When electrons and holes are selectively consumed on different surfaces, a charge separation is therefore promoted by the formation of a concentration gradient, and the recombination becomes less frequent.[27] The flux method is one of the crystal growth techniques that allows one to grow crystals with high crystallinity and idiomorphic shape from a supersaturated high-temperature melt with the assistance of a flux (molten salts or metals). There are some certain criteria for selecting a good flux, and the most critical ones are high solubility of the reagents in the flux and a significant change in the solubility with temperature.[28] For instance, the (110) layered perovskite $La_2Ti_2O_7$ crystals were grown with high purity and homogeneous microstructures using the sulfate (Na_2SO_4/K_2SO_4)[29] and chloride (NaCl/KCl)[30] fluxes. The alkali-metal molybdates are also attractive for oxide crystal growth because of their ability to dissolve oxide reagents and reduced volatility. In addition, the sodium and potassium salts are water-soluble, which can easily be separated later from the grown crystal product, and have low melting points, low volatility, low viscosity, and exceptionally fast dissolution kinetics.[31] Using the alkali-metal molybdate flux, substitution in the grown crystals may also be negligible because of the high oxidation state of molybdenum.[29] The growth of $La_2Ti_2O_7$ crystals in the alkali-metal molybdate flux and their conversion to $LaTiO_2N$ crystals have not been reported yet. In this work, we therefore put emphasis on the study of the effect of the alkali-metal molybdate flux on the growth of $La_2Ti_2O_7$ crystals, the crystal growth manner, and their nitridability to form $LaTiO_2N$ crystals under a high-temperature NH_3 atmosphere.

2. EXPERIMENTAL SECTION

2.1. Flux Growth of $La_2Ti_2O_7$ Crystals. Reagent-grade La_2O_3, TiO_2, $Na_2MoO_4{\cdot}2H_2O$, K_2MoO_4, and NaCl (Wako Pure Chemical Industries, Ltd.) were used as received for alkali-metal molybdate flux growth of the $La_2Ti_2O_7$ crystals. The detailed experimental conditions for alkali-metal molybdate flux growth of the $La_2Ti_2O_7$ crystals are given in Table 1. In this work, a stoichiometric mixture of La_2O_3 and TiO_2 (molar ratio = 1:2) was used as the solute, and Na_2MoO_4, K_2MoO_4, NaCl, and mixed NaCl + K_2MoO_4 (3:7) were employed as the flux. The solute concentration was varied from 1 to 20 mol %, and the total mass of a solute-flux mixture was approximately 10 g for each run. After being well homogenized for 30 min, each solute-flux mixture was put into a platinum crucible with a capacity of 30 cm^3, and a platinum lid was loosely closed. The mixture-containing platinum crucible was then placed in an electric furnace, heated to 1100 °C at a heating rate of 200 °C h^{-1}, and held at that temperature for 10 h. Subsequently, the platinum crucible was cooled to 500 °C at a cooling rate of 50 °C h^{-1} using a cooling control program and then allowed to cool naturally to room temperature. The flux-grown $La_2Ti_2O_7$ crystals were separated from the remaining flux by washing the grown crystal products with hot water and dried at 100 °C for 12 h. To investigate the effect of the alkali-metal chloride and alkali-metal chloride–molybdate fluxes on the growth of $La_2Ti_2O_7$ crystals, additional parallel experiments were performed using the NaCl and mixed NaCl + K_2MoO_4 fluxes at 1000 °C for 10 h, at a heating rate of 100 °C h^{-1} and cooling rates of 50 and 150 °C h^{-1} to 500 °C, respectively.

DOI: 10.1021/ic502862t
Inorg. Chem. 2015, 54, 3237–3244

2.2. Fabrication of $LaTiO_2N$ Crystals. To fabricate the $LaTiO_2N$ crystals, 0.5 g of the flux-grown $La_2Ti_2O_7$ crystals was wrapped with quartz wool, placed in a vertical tubular furnace with a quartz rod, nitride at 950 °C for 15 h at a heating rate of 10 °C min^{-1} under an NH_3 flow (200 mL min^{-1}), and cooled naturally to room temperature.

2.3. Characterization. The crystal phases formed were identified by X-ray diffraction (XRD; MiniflexII, Rigaku) with Cu Kα radiation (λ = 0.154 nm). The X-ray diffractometer was operated at 30 kV and 20 mA in the 2θ range from 5° to 80°. The elemental compositions of the crystal products were analyzed by inductively coupled plasma optical emission spectrometry (ICP-OES; SPS5510, SII), energy-dispersive X-ray spectroscopy (EDS; JSM-6710F, JEOL), and X-ray photoelectron spectroscopy (XPS; JPS-9010MC, JEOL) using non-monochromated Mg Kα radiation (1253.6 eV) with a 10 mA emission current and a 10 kV acceleration voltage. The XPS profiles were fitted using a Gaussian−Lorentzian function, and the peak positions were normalized by positioning the C 1s peak at 284.5 eV. The morphologies and sizes of the flux-grown crystals were examined by scanning electron microscopy (SEM; JCM-5700, JEOL) at an acceleration voltage of 15 kV. The average sizes of the crystals grown were estimated by an intercept technique using SEM micrographs on at least 200 selected crystals. The crystallinity and developed facets of the flux-grown crystals were analyzed by high-resolution transmission electron microscopy (TEM; JEM-2010, JEOL) operating at 200 kV. The ultraviolet−visible (UV−vis) diffuse-reflectance spectra of the crystal products were recorded on a JASCO V-670 spectrophotometer.

3. RESULTS AND DISCUSSION

To study the effect of the solute concentration on the growth of $La_2Ti_2O_7$ crystals using the alkali-metal molybdate fluxes, the solute concentration was varied from 1 to 20 mol %. Parts a and b of Figure 2 show the XRD patterns of the crystals grown using the Na_2MoO_4 and K_2MoO_4 fluxes and the International Centre for Diffraction Data Powder Diffraction File (ICDD PDF) data for $La_2Ti_2O_7$ (ICDD PDF 28-0517). All of the diffraction lines can be indexed to the monoclinic phase of $La_2Ti_2O_7$ (ICDD PDF 28-0517) with lattice parameters of a = 13.0150 Å, b = 5.5456 Å, and c = 7.8170 Å. No diffraction lines belonging to the impurity phases were detected, implying that the phase-pure $La_2Ti_2O_7$ crystals could be grown with different solute concentrations using the Na_2MoO_4 and K_2MoO_4 fluxes. Intense and sharp diffraction lines were observed in the XRD patterns of the flux-grown crystals, indicating a high degree of crystallinity. The diffraction lines resulting from the {100} plane of the $La_2Ti_2O_7$ crystals are clearly stronger compared to the corresponding lines of the ICDD PDF data, evidencing dominance of the {100} plane in the $La_2Ti_2O_7$ crystals grown using the alkali-metal molybdate fluxes. Upon an increase in the solute concentration, the intensity of other diffraction lines of the $La_2Ti_2O_7$ crystals slowly increased because of the development of other crystal faces through the flux growth process.

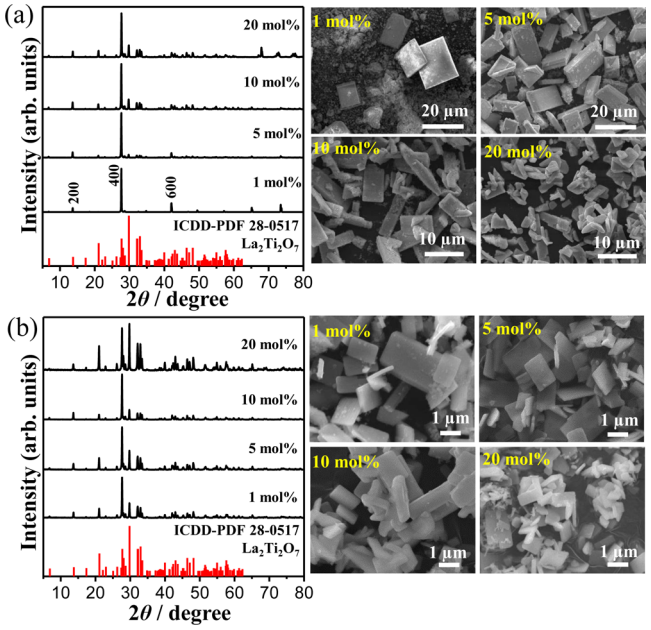

Figure 2. XRD patterns and SEM images of the $La_2Ti_2O_7$ crystals grown using the (a) Na_2MoO_4 and (b) K_2MoO_4 fluxes with different solute concentrations.

Parts a and b of Figure 2 show the SEM images of the crystals grown using the Na_2MoO_4 and K_2MoO_4 fluxes. It is clear that the crystal shape and size were significantly affected by the solute concentration. As shown in Figure 2a, the crystals grown with a solute concentration of 1 mol % using the Na_2MoO_4 flux have an elongated platelet shape (ca. 29.3 μm in length and ca. 18.6 μm in width) along with agglomerated small particles, whereas using the solute concentration of 5 mol % advanced the growth of uniform platelet microstructures (ca. 12.8 μm in length and ca. 6.2 μm in width) with well-developed crystal faces. Further increases in the solute concentration to 10 and 20 mol % lead to the growth of irregular crystals with some platelets (ca. 8.4 μm in length and ca. 3.7 μm in width) and irregular crystals (ca. 2.6 μm in length and ca. 1.8 μm in width), respectively. Using the K_2MoO_4 flux, $La_2Ti_2O_7$ crystals in the platelet shape were grown (Figure 2b). When the solute concentration was increased from 1 to 20 mol %, the average length and width of the crystals decreased without considerable alteration of the overall crystal morphology, as follows: 1.23 and 0.76 μm (1 mol %) < 1.21 and 0.68 μm (5 mol %) < 1.08 and 0.58 μm (10 mol %) < 0.96 and 0.57 μm (20 mol %). Judging from the SEM results, the solute concentration of 5 mol % appears to be optimum for the growth of the $La_2Ti_2O_7$ crystals with uniform shape and size using the Na_2MoO_4 and K_2MoO_4 fluxes. As shown in Figure 3a,b, the average size of the $La_2Ti_2O_7$ crystals grown using the Na_2MoO_4 flux is much larger than that of the $La_2Ti_2O_7$ crystals grown using the K_2MoO_4 flux probably because of a high degree of supersaturation and high solubility of the solute in the Na_2MoO_4 flux compared to the K_2MoO_4 flux, allowing the growth of larger $La_2Ti_2O_7$ crystals with well-developed crystal faces.[32] In addition, monovalent cations (Na^+ and K^+) can additionally decrease the viscosity of the melt by preventing network formation in melts.[28] With an increase in

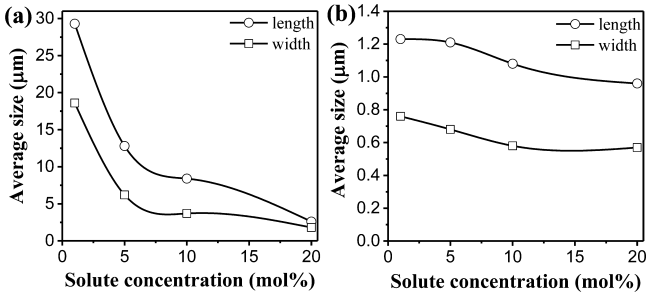

Figure 3. Average size of the $La_2Ti_2O_7$ crystals grown using the (a) Na_2MoO_4 and (b) K_2MoO_4 fluxes as a function of the solute concentration.

DOI: 10.1021/ic502862t
Inorg. Chem. 2015, 54, 3237−3244

the solute concentration from 1 to 20 mol %, the average size of the $La_2Ti_2O_7$ crystals grown using the Na_2MoO_4 and K_2MoO_4 fluxes decreased. This is because the solute with lower concentration was easily soluble in the alkali-metal molybdate fluxes, inducing the growth of larger crystals, whereas smaller crystals were grown because of a large number of nuclei in the supersaturated high-temperature melt, hindering the complete growth of those small crystals.[33]

The crystallographic characteristics of the $La_2Ti_2O_7$ crystals grown with a solute concentration of 5 mol % using the Na_2MoO_4 and K_2MoO_4 fluxes were examined by TEM, and the results are shown in Figure 4. The magnified bright-field TEM

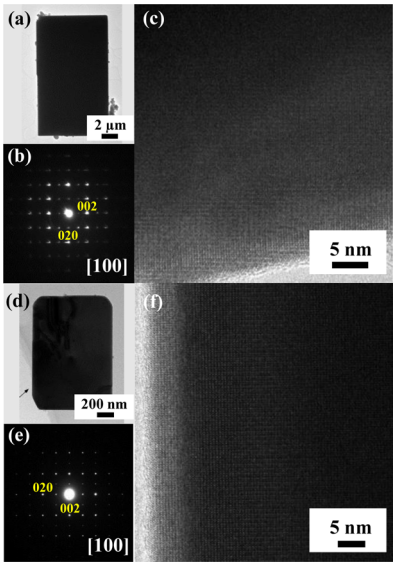

Figure 4. TEM images, SAED patterns, and high-resolution TEM images of the $La_2Ti_2O_7$ crystals grown using the (a–c) Na_2MoO_4 and (d–f) K_2MoO_4 fluxes with a 5 mol % solute concentration.

images (Figure 4a,d) confirm that the $La_2Ti_2O_7$ crystals grown using the Na_2MoO_4 and K_2MoO_4 fluxes are elongated and rounded rectangular-shaped platelets, respectively, which is consistent with the SEM observations. In Figure 4b,e, highly ordered selected-area electron diffraction (SAED) spots of individual $La_2Ti_2O_7$ platelets grown using the Na_2MoO_4 and K_2MoO_4 fluxes reveal their single-crystalline nature. In the SAED patterns, the d_{002} and d_{020} spacings were determined to be 0.387 and 0.278 nm, respectively, which are in good agreement with the theoretical values of d_{002} = 0.386 and d_{020} = 0.277 nm. The corresponding diffraction spots indexed as 002 and 020 reflections corroborate the preferred ⟨010⟩ and ⟨001⟩ growth directions of the $La_2Ti_2O_7$ platelets grown using the Na_2MoO_4 and K_2MoO_4 fluxes along the *b* and *c* axes, respectively. After analysis of the surfaces and cross sections of the (100) and (010) planes of the idealized crystal structure of $La_2Ti_2O_7$, shown in Figure S1 in the Supporting Information (SI), no significant difference was found in the *b* and *c* axes. Nevertheless, the Na_2MoO_4 and K_2MoO_4 fluxes promoted growth of the $La_2Ti_2O_7$ platelet crystals along the *b* and *c* axes, respectively. The lattice images of the $La_2Ti_2O_7$ crystals, shown in Figure 4c,f, were taken with the incident beam along the [100] direction. No obvious defects were observed in these lattice images, confirming the high crystallinity of the $La_2Ti_2O_7$ crystals grown using the Na_2MoO_4 and K_2MoO_4 fluxes.

It is known that the morphology of crystals grown using the flux strongly depends on a number of factors, including solute–solvent interaction and the crystal–solution interface; however, there is so far no generalized flux growth mechanism. For the alkali-metal molybdate flux growth of two-dimensional $La_2Ti_2O_7$ platelet crystals, here we briefly postulate the growth manner based on the obtained but limited results. First, the layered monoclinic crystal structure and the feeble bonding between the layers play important roles in the growth of two-dimensional $La_2Ti_2O_7$ crystals using the flux. In the monoclinic crystal structure of $La_2Ti_2O_7$, the layers are built from the (110) perovskite slabs composed of corner-sharing TiO_6 octahedra and coordinated lanthanum cations.[34] In addition to the degree of supersaturation, another reason for growing two-dimensional $La_2Ti_2O_7$ platelet crystals with an exposed {100} face appears to be the difference in the growth rate of the planes. That is, while crystal growth was preferred along the ⟨010⟩ and ⟨001⟩ directions, crystal growth along the ⟨100⟩ direction was relatively slow. Therefore, the {100} face became the most prominent on the $La_2Ti_2O_7$ platelet crystals grown using the Na_2MoO_4 and K_2MoO_4 fluxes. Moreover, the polar {010} and {001} planes could also provide a smooth transition between the crystal and the melt, thus decreasing the free surface energy.[35] Afanasiev[36] also described that, if a crystalline structure contains charged planes populated with alkali-metal cations, such planes will be preferentially exposed in the crystal product. Similarly, anionic charged planes can also be favored.[37] We assume that the Burton–Cabrera–Frank (BCF)-type screw-dislocation process was probably involved in the growth of the $La_2Ti_2O_7$ platelet crystals. In the high-temperature melt, the growth rate of crystals is believed to be governed by the rate of ions diffusing to kinks in the steps of spirals. Although crystal growth from the fluxes is generally considered to be a BCF-type screw-dislocation process,[28,38] oriented attachment and a Kirkendall effect[36] and layer-by-layer growth[39] have also recently been reported.

Next, we investigated the effect of the cooling rate on the morphology of the $La_2Ti_2O_7$ crystals grown using the Na_2MoO_4 and K_2MoO_4 fluxes. The results are shown in Figure 5. Using the Na_2MoO_4 flux, the $La_2Ti_2O_7$ crystals were

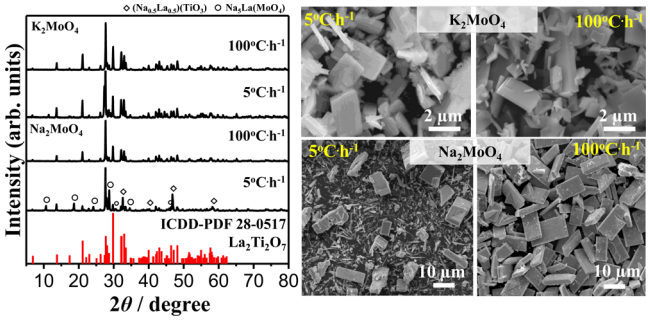

Figure 5. XRD patterns and SEM images of the $La_2Ti_2O_7$ crystals grown using the Na_2MoO_4 and K_2MoO_4 fluxes with a 5 mol % solute concentration at cooling rates of 5 and 100 °C h^{-1}.

grown along with the $Na_{0.5}La_{0.5}TiO_3$ (ICDD PDF 89-6954) and Na_5LaMoO_4 (ICDD PDF 72-2158) phases at a cooling rate of 5 °C h^{-1}. Interestingly, the formation of these two impurity phases was suppressed by a cooling rate of 100 °C h^{-1}, as shown in the XRD patterns. In contrast to the Na_2MoO_4 flux, the K_2MoO_4 flux did not show such a cooling-rate-dependent effect on the growth of the $La_2Ti_2O_7$ crystals. That

DOI: 10.1021/ic502862t
Inorg. Chem. 2015, 54, 3237–3244

is, using the K_2MoO_4 flux, single-phase $La_2Ti_2O_7$ crystals were grown at a cooling rate of 5 °C h^{-1} as well as 100 °C h^{-1}. The formation of sodium- and molybdenum-containing impurity phases in the crystal product grown using the Na_2MoO_4 flux at a cooling rate of 5 °C h^{-1} was thought to be due to the high reactivity of the Na_2MoO_4 flux, compared to the K_2MoO_4 flux, in which Na^+ and Mo^{6+}/Mo^{5+} could easily react with La^{3+} to form the Na_5LaMoO_4 phase. Because of a good six-coordinated effective ionic radius matching between Mo^{6+} (0.62 Å) and Ti^{4+} (0.605 Å),[40] the Mo^{6+} ions were prone to replace Ti^{4+} in the lattice, resulting in the Na_5LaMoO_4 phase. The $Na_{0.5}La_{0.5}TiO_3$ phase was formed because of partial substitution of La^{3+} by Na^+ from the Na_2MoO_4 flux in the lattice because the ionic radius of La^{3+} (1.16 Å) is very close to that of Na^+ (1.18 Å).[41] The SEM images in Figure 5 confirm that the $La_2Ti_2O_7$ crystals with nearly identical platelet shape and size (ca. 17.3 μm) were grown using the K_2MoO_4 flux regardless of the difference in the cooling rates. Using the Na_2MoO_4 flux, large pseudocubic $La_2Ti_2O_7$ crystals (ca. 8.4 μm) were grown along with acicular (ca. 7.1 μm) and irregular (ca. 10.2 μm) crystals of Na_5LaMoO_4 and $Na_{0.5}La_{0.5}TiO_3$ at a cooling rate of 5 °C h^{-1}, whereas large $La_2Ti_2O_7$ platelet crystals were grown at a cooling rate of 100 °C h^{-1}. It can be concluded that the K_2MoO_4 flux did not have a cooling-rate-dependent effect on the growth of the $La_2Ti_2O_7$ crystals compared to the Na_2MoO_4 flux owing to the evaporation of the flux rather than cooling.

Conversion of the $La_2Ti_2O_7$ crystals to the $LaTiO_2N$ crystals was also examined in this study by nitriding the four $La_2Ti_2O_7$ samples, grown separately using the Na_2MoO_4, K_2MoO_4, NaCl, and mixed NaCl + K_2MoO_4 fluxes, at 950 °C for 15 h under an NH_3 flow. The XRD patterns and SEM images of the samples before and after nitridation are compiled in Figures 6 and 7.

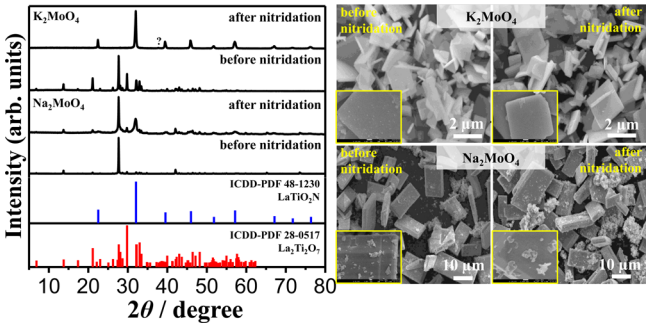

Figure 6. XRD patterns and SEM images of the $La_2Ti_2O_7$ crystals grown using the Na_2MoO_4 and K_2MoO_4 fluxes with a 5 mol % solute concentration before and after nitridation under an NH_3 flow (200 mL min^{-1}) at 950 °C for 15 h.

The XRD patterns clearly indicate that the phase-pure $La_2Ti_2O_7$ crystals could be grown using the Na_2MoO_4, K_2MoO_4, NaCl, and mixed NaCl + K_2MoO_4 fluxes; however, their crystal morphologies were strongly dependent on the flux used. As shown in Figure 6, uniform platelets (ca. 12.8 μm in length and ca. 6.2 μm in width) with well-developed crystal faces were grown using the Na_2MoO_4 flux, whereas the $La_2Ti_2O_7$ platelet crystals with ca. 1.21 μm in length and ca. 0.68 μm in width were grown using the K_2MoO_4 flux. Acicular and platelet $La_2Ti_2O_7$ crystals with average sizes of 2.8 and 3.7 μm were grown using the NaCl and mixed NaCl + K_2MoO_4 fluxes, respectively (Figure 7). Interestingly, high-temperature transformation of the $La_2Ti_2O_7$ crystals into the $LaTiO_2N$

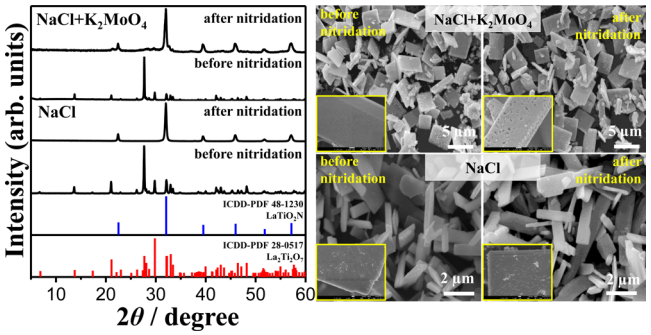

Figure 7. XRD patterns and SEM images of the $La_2Ti_2O_7$ crystals grown using the NaCl and mixed NaCl + K_2MoO_4 fluxes with a 5 mol % solute concentration before and after nitridation under an NH_3 flow (200 mL min^{-1}) at 950 °C for 15 h.

crystals under an NH_3 atmosphere proceeded without considerable alteration of the overall crystal morphology, including the length and width. In addition, the surface morphology of the crystals grown using the Na_2MoO_4 and K_2MoO_4 fluxes did not change significantly even after high-temperature nitridation under an NH_3 atmosphere. On the contrary, the surface morphology of the crystals grown using the NaCl and NaCl + K_2MoO_4 fluxes was, in fact, influenced by the nitridation process, leading to the formation of porous crystals and the segregation of small crystal structures. Namely, the crystals grown using the NaCl flux became porous crystal structures because of the larger lattice strain accumulation upon structural transformation from $La_2Ti_2O_7$ to $LaTiO_2N$, whereas small crystals started to segregate on the surface of the platelet crystals grown using the NaCl + K_2MoO_4 flux, as shown in Figures 6 and 7. Considering the XRD results, the formability of the $LaTiO_2N$ crystals from the precursor $La_2Ti_2O_7$ crystals was appreciably reliant on the flux used to grow the $La_2Ti_2O_7$ crystals. That is, the $La_2Ti_2O_7$ crystals grown using the K_2MoO_4 and NaCl fluxes were nearly completely converted into the $LaTiO_2N$ crystals (with an unidentified XRD peak at $2\theta = 37°$ in Figure 6), while conversion of the $La_2Ti_2O_7$ crystals grown using the Na_2MoO_4 and mixed NaCl + K_2MoO_4 fluxes to the $LaTiO_2N$ crystals seems to be not completed yet even after nitridation at 950 °C for 15 h under an NH_3 atmosphere. It is believed that incomplete conversion of the $La_2Ti_2O_7$ crystals to the $LaTiO_2N$ crystals was somehow associated with the simultaneous presence of Na^+ and Mo^{6+}/Mo^{5+} from the flux in a high-temperature solution. For comparison reasons, $La_2Ti_2O_7$ was also produced in sintered pellet form with thicknesses of 1.2 and 3.6 mm by a flux-free solid-state process at 1300 °C for 12 h and nitrided at 950 °C for 10 h under an NH_3 atmosphere (200 mL min^{-1}). The results shown in Figures S5 and S6 in the SI evidence that the $La_2Ti_2O_7$ pellet with a thickness of 1.2 mm was partially converted to $LaTiO_2N$, whereas the $La_2Ti_2O_7$ pellet with a thickness of 3.6 mm was not converted to $LaTiO_2N$ owing to the thickness of the pellet and the larger size of the crystals.

We assume that there are mainly two factors, namely, the crystal size and unintentional impurity in the $La_2Ti_2O_7$ crystal lattice, negatively affecting complete conversion of the $La_2Ti_2O_7$ crystals to the $LaTiO_2N$ crystals under high-temperature nitridation using NH_3. As the nitridation process slowly advances from the surface to the bulk, the crystal size becomes critical to the completion of the oxide-to-oxynitride transformation. As shown in Figures 6 and 7, the $La_2Ti_2O_7$

DOI: 10.1021/ic502862t
Inorg. Chem. 2015, 54, 3237−3244

crystals grown using the Na_2MoO_4 and mixed NaCl + K_2MoO_4 fluxes are in the form of platelets with ca. 12.8 μm length and ca. 6.2 μm width and with an average size of 3.7 μm, respectively. Compared to the $La_2Ti_2O_7$ crystals grown with smaller sizes using the K_2MoO_4 and NaCl fluxes (Figures 6 and 7), these larger $La_2Ti_2O_7$ crystals are thought to be the reason for incomplete conversion of the $La_2Ti_2O_7$ crystals to the $LaTiO_2N$ crystals within 15 h of nitridation at 950 °C using NH_3. Ebbinghaus et al.[42] reported that the formation of a perovskite $LaTiO_2N$ layer was basically restricted to the surface (2−3 μm) of the $La_2Ti_2O_7$ crystal slice after long nitridation, and the thickness of the $LaTiO_2N$ layer depended strongly on the nitridation time. Mo^{6+} easily undergoes reduction by accepting electrons, especially under a high-temperature NH_3 atmosphere. Therefore, a change in the valence state of Mo from Mo^{6+} to Mo^{5+}, which can either substitutionally replace Ti^{4+} or enter into the interstitial positions because of a small difference in their ionic radii, was possible. Also, La^{3+} was unintentionally partially replaced by Na^+ from the flux because of the similarity in their ionic radii. Because of the similarity in their ionic radii, the diffraction peak positions of the $La_2Ti_2O_7$ crystals remained unchanged even upon the unintentional introduction of the molybdenum and sodium species in the crystal lattice. In addition, the amount of Na^+ and Mo^{6+}/Mo^{5+} introduced into the $La_2Ti_2O_7$ crystal lattice was considerably small. Unintentional doping of $La_2Ti_2O_7$ with molybdenum because of the similarity in the ionic radii of Mo^{6+} and Ti^{4+} is likely to lead to incomplete conversion of $La_2Ti_2O_7$ to $LaTiO_2N$. One may wonder why then conversion of the $La_2Ti_2O_7$ crystals grown using the K_2MoO_4 flux to the $LaTiO_2N$ crystals was nearly completed. Compared to the K_2MoO_4 and NaCl fluxes, the introduction of an excess amount of molybdenum and sodium into the $La_2Ti_2O_7$ crystals using the Na_2MoO_4 and mixed NaCl + K_2MoO_4 fluxes was confirmed by elemental analysis. The ICP-OES and XPS results are shown in Figures S2 and S3 in the SI. The results of elemental mapping of the $La_2Ti_2O_7$ crystals at the microstructural level by SEM with EDS are also shown in Figure S4 in the SI. As shown, the $La_2Ti_2O_7$ crystals grown using the Na_2MoO_4 and mixed NaCl + K_2MoO_4 fluxes possess higher amounts of sodium (22.5 and 2.0 atom %) and molybdenum (11.5 and 2.5 atom %) in comparison to the $La_2Ti_2O_7$ crystals grown using the K_2MoO_4 and NaCl fluxes (sodium, 0.0 and 1.2 atom %; molybdenum, 0.7 and 0.0 atom %). Therefore, it is believed that an excess amount of molybdenum with higher valence could substitutionally replace titanium and also enter into the interstitial positions. A substitutional form of doping of titanium with molybdenum having a valence change under a reductive NH_3 atmosphere may increase the oxygen vacancy level, promoting phase transformation through lattice relaxation. In contrast, an interstitial form of doping of titanium with molybdenum may enhance lattice constraint, delaying phase transformation. As shown in Figures S2−S4 in the SI, compared to the NaCl + K_2MoO_4 flux, a higher amount of molybdenum was introduced, using the Na_2MoO_4 flux, into $La_2Ti_2O_7$ in the form of an interstitial dopant, enhancing the structural stability. Hence, further prolongation of the nitridation time and/or an increase in the nitridation temperature may possibly allow completion of the conversion of larger $La_2Ti_2O_7$ crystals to the $LaTiO_2N$ crystals, but at the same time, it may also evoke increased defect formation. In addition, a decrease in the photocatalytic efficiency with an excess amount of molybdenum in the $La_2Ti_2O_7$ because of the created mid band gaps, which act as recombination centers, should also be taken into account.[43] A slight change in the tolerance factor and octahedral tilting by the introduction of unintentional dopants (sodium and molybdenum) in the $La_2Ti_2O_7$ cannot be completely ignored to interpret the contribution of unintentional impurities upon incompletion of the $La_2Ti_2O_7$-to-$LaTiO_2N$ transformation under nitridation using NH_3 at 950 °C for 15 h. However, further studies need to be performed to confirm this.

Figure 8 shows the UV−vis diffuse-reflectance spectra of the $La_2Ti_2O_7$ crystals grown using the K_2MoO_4 flux and the

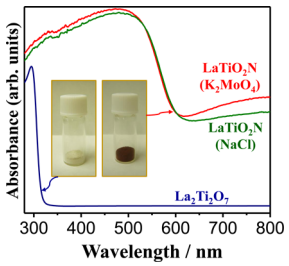

Figure 8. UV−vis diffuse-reflectance spectra of the $La_2Ti_2O_7$ crystals grown using the K_2MoO_4 flux (blue) and the $LaTiO_2N$ crystals fabricated by nitridation of the $La_2Ti_2O_7$ crystals grown using the NaCl (green) and K_2MoO_4 (red) fluxes under an NH_3 flow (200 mL min^{-1}) at 950 °C for 15 h.

$LaTiO_2N$ crystals fabricated by nitridation of the $La_2Ti_2O_7$ crystals grown using the NaCl and K_2MoO_4 fluxes. The UV−vis diffuse-reflectance spectra were measured and converted to absorption spectra using the Kubelka−Munk function. As shown in Figure 8, the $La_2Ti_2O_7$ crystals grown using the K_2MoO_4 flux show a strong absorption in the UV region, and the absorption edge wavelength is estimated to be approximately 320 nm. In the UV−vis diffuse-reflectance spectra of the $LaTiO_2N$ crystals fabricated by nitridation of the $La_2Ti_2O_7$ crystals grown using the NaCl and K_2MoO_4 fluxes, an onset of the light absorption characteristics of the band-gap excitation of $LiTaO_2N$ with a distinctive reddish-brownish color is noticed at around 600 nm. The absorption edge shift was caused by the valence-band shift from O 2p for $La_2Ti_2O_7$ to N 2p for $LaTiO_2N$. The $LaTiO_2N$ crystals also exhibited a strong background absorption beyond the absorption edge wavelength, which is generally attributed to the presence of defects associated with the reduced Ti^{3+} species.[20,44] Compared to the $LaTiO_2N$ crystals fabricated by nitridation of the $La_2Ti_2O_7$ crystals grown using the NaCl flux, the $LaTiO_2N$ crystals fabricated by nitridation of the $La_2Ti_2O_7$ crystals grown using the K_2MoO_4 flux showed higher background absorption intensity in the longer wavelength because of the reduced molybdenum species partially introduced unintentionally in the $LaTiO_2N$ crystal lattice. The optical band-gap energy was estimated from the UV−vis diffuse-reflectance spectra using the Kubelka−Munk function. The $La_2Ti_2O_7$ and $LaTiO_2N$ crystals have band gaps of approximately 3.8 and 2.1 eV, respectively. Note that the $LaTiO_2N$ crystals fabricated by nitridation of the $La_2Ti_2O_7$ crystals grown using the K_2MoO_4 and NaCl fluxes have almost no significant difference in their band-gap energy. The $LaTiO_2N$ crystals fabricated by nitridation of the $La_2Ti_2O_7$ crystals grown using the K_2MoO_4 and NaCl fluxes should be suitable for the direct solar water splitting reaction with photoelectochemical cells.

DOI: 10.1021/ic502862t
Inorg. Chem. 2015, 54, 3237−3244

4. CONCLUSIONS

Here we demonstrated the flux growth of the $La_2Ti_2O_7$ crystals using the Na_2MoO_4, K_2MoO_4, NaCl, and mixed NaCl + K_2MoO_4 fluxes and their nitridability to form the $LaTiO_2N$ crystals under a high-temperature NH_3 atmosphere. An increase in the solute concentration led to a decrease of the average size of the $La_2Ti_2O_7$ crystals without considerable alteration of the overall crystal morphology. The K_2MoO_4 flux did not show a cooling-rate-dependent effect on the growth of the $La_2Ti_2O_7$ crystals in comparison to the Na_2MoO_4 flux. The $La_2Ti_2O_7$ crystals with the preferred ⟨010⟩ and ⟨001⟩ growth directions along the *b* and *c* axes were grown using the Na_2MoO_4 and K_2MoO_4 fluxes, respectively. It was found that conversion of the $La_2Ti_2O_7$ crystals to the $LaTiO_2N$ crystals was strongly dependent on the flux used to grow the precursor $La_2Ti_2O_7$ crystals. Compared to the $La_2Ti_2O_7$ crystals grown using the K_2MoO_4 and NaCl fluxes, conversion of the $La_2Ti_2O_7$ crystals grown using the Na_2MoO_4 and NaCl + K_2MoO_4 fluxes to the $LaTiO_2N$ crystals seemed to be not completed yet even after nitridation at 950 °C for 15 h using NH_3 because of the larger crystal size and the presence of unintentional impurities (sodium and molybdenum from the flux) in the $La_2Ti_2O_7$ crystal lattice. The obtained results suggested that the K_2MoO_4 and NaCl fluxes were favorable to grow the $La_2Ti_2O_7$ crystals with acicular and platelet shapes and were nearly completely converted to the $LaTiO_2N$ crystals. The $LaTiO_2N$ crystals fabricated by nitridation of the $La_2Ti_2O_7$ crystals grown using the K_2MoO_4 and NaCl fluxes should be suitable for direct solar water splitting.

■ ASSOCIATED CONTENT

Supporting Information

Surfaces and cross sections of the (100) and (010) planes of the idealized crystal structure of $La_2Ti_2O_7$, ICP-OES, XPS, and EDS results of $La_2Ti_2O_7$ crystals grown using the Na_2MoO_4, K_2MoO_4, NaCl, and mixed NaCl + K_2MoO_4 fluxes, and XRD patterns and SEM images of the $La_2Ti_2O_7$ pellets produced by a flux-free solid-state process before and after nitridation at 950 °C for 10 h under an NH_3 atmosphere. This material is available free of charge via the Internet at http://pubs.acs.org.

■ AUTHOR INFORMATION

Corresponding Author

*E-mail: teshima@shinshu-u.ac.jp.

Author Contributions

The manuscript was written through the equal contribution of all authors. All authors have given approval to the final version of the manuscript.

Notes

The authors declare no competing financial interest.

■ ACKNOWLEDGMENTS

This research was partially supported by the Japan Technological Research Association of Artificial Photosynthetic Chemical Process (ARPChem). The authors thank Mr. Kenta Kawashima for performing supplemental experiments.

■ REFERENCES

(1) Ishizawa, N.; Marumo, F.; Iwai, S.; Kimura, M.; Kawamura, T. *Acta Crystallogr., Sect. B* **1982**, *38*, 368−372.

(2) Herrera, G.; Jiménez-Mier, J.; Chavira, E. *Mater. Charact.* **2014**, *89*, 13−22.

(3) Schmalle, H. W.; Williams, T.; Reller, A.; Linden, A.; Bednorz, J. G. *Acta Crystallogr., Sect. B* **1993**, *49*, 235−244.

(4) Hwang, D. W.; Lee, J. S.; Li, W.; Oh, S. H. *J. Phys. Chem. B* **2003**, *107*, 4963−4970.

(5) Yamamoto, J. K.; Bhalla, A. S. *J. Appl. Phys.* **1991**, *70*, 4469−4471.

(6) Atuchin, V. V.; Gavrilova, T. A.; Grivel, J. C.; Kesler, V. G. *J. Phys. D: Appl. Phys.* **2009**, *42*, 35305−35310.

(7) Kim, W. S.; Ha, S. M.; Yun, S.; Park, H. H. *Thin Solid Films* **2002**, *420*−*421*, 575−578.

(8) Kim, W. S.; Ha, S. M.; Yang, J. K.; Park, H. H. *Thin Solid Films* **2001**, *398*−*399*, 663−667.

(9) Kimura, M.; Nanamatsu, S.; Doi, K.; Matsushita, S.; Takahashi, M. *Jpn. J. Appl. Phys.* **1972**, *11*, 904.

(10) Fasquelle, D.; Carru, J. C.; Le Gendre, L.; Le Paven, C.; Pinel, J.; Cheviré, F.; Tessier, F.; Marchand, R. *J. Eur. Ceram. Soc.* **2005**, *25*, 2085−2088.

(11) Nanamatsu, S.; Kimura, M.; Doi, K.; Matsushita, S.; Yamada, N. *Ferroelectrics* **1974**, *8*, 511−513.

(12) Diallo, P. T.; Boutinaud, P.; Mahiou, R. *J. Alloys Compd.* **2002**, *341*, 139−143.

(13) Kim, H. G.; Hwang, D. W.; Kim, J.; Kim, Y. G.; Lee, J. S. *Chem. Commun.* **1999**, 1077−1078.

(14) Ando, T.; Wakamatsu, T.; Masuda, K.; Yoshida, N.; Suzuki, K.; Masutani, S.; Katayama, I.; Uchida, H.; Hirose, H.; Kamimoto, A. *Appl. Surf. Sci.* **2009**, *255*, 9688−9690.

(15) Abe, R.; Higashi, M.; Sayama, K.; Abe, Y.; Sugihara, H. *J. Phys. Chem. B* **2006**, *110*, 2219−2226.

(16) Hojamberdiev, M.; Zhu, G.; Sujaridworakun, P.; Jinawath, S.; Liu, P.; Zhou, J.-P. *Powder Technol.* **2012**, *218*, 140−148.

(17) Ruzimuradov, O.; Nurmanov, S.; Hojamberdiev, M.; Prasad, R. M.; Gurlo, A.; Broetz, J.; Nakanishi, K.; Riedel, R. *J. Eur. Ceram. Soc.* **2014**, *34*, 809−816.

(18) Yashima, M.; Saito, M.; Nakano, H.; Takata, T.; Ogisu, K.; Domen, K. *Chem. Commun.* **2010**, *46*, 4704−4706.

(19) Kasahara, A.; Nukumizu, K.; Hitoki, G.; Takata, T.; Kondo, J. N.; Hara, M.; Kobayashi, H.; Domen, K. *J. Phys. Chem. A* **2002**, *106*, 6750−6753.

(20) Kasahara, A.; Nukumizu, K.; Takata, T.; Kondo, J. N.; Hara, M.; Kobayashi, H.; Domen, K. *J. Phys. Chem. B* **2003**, *107*, 791−797.

(21) Maegli, A. E.; Pokrant, S.; Hisatomi, T.; Trottmann, M.; Domen, K.; Weidenkaff, A. *J. Phys. Chem. C* **2014**, *118*, 16344−16351.

(22) Leroy, C. M.; Maegli, A. E.; Sivula, K.; Hisatomi, T.; Xanthopoulos, N.; Otal, E. H.; Yoon, S.; Weidenkaff, A.; Sanjines, R.; Gratzel, M. *Chem. Commun.* **2012**, *48*, 820−822.

(23) Feng, J.; Luo, W.; Fang, T.; Lv, H.; Wang, Z.; Gao, J.; Liu, W.; Yu, T.; Li, Z.; Zou, Z. *Adv. Funct. Mater.* **2014**, *24*, 3535−3542.

(24) Minegishi, T.; Nishimura, N.; Kubota, J.; Domen, K. *Chem. Sci.* **2013**, *4*, 1120−1124.

(25) Matsukawa, M.; Ishikawa, R.; Hisatomi, T.; Moriya, Y.; Shibata, N.; Kubota, J.; Ikuhara, Y.; Domen, K. *Nano Lett.* **2014**, *14*, 1038−1041.

(26) Nishimura, N.; Raphael, B.; Maeda, K.; Le Gendre, L.; Abe, R.; Kubota, J.; Domen, K. *Thin Solid Films* **2010**, *518*, 5855−5859.

(27) Moriya, Y.; Takata, T.; Domen, K. *Coord. Chem. Rev.* **2013**, *257*, 1957−1969.

(28) Bugaris, D. E.; zur Loye, H. C. *Angew. Chem., Int. Ed.* **2012**, *51*, 3780−3811.

(29) Arney, D.; Porter, B.; Greve, B.; Maggard, P. A. *J. Photochem. Photobiol. A: Chem.* **2008**, *199*, 230−235.

(30) Wagata, H.; Zettsu, N.; Yamaguchi, A.; Nishikori, H.; Yubuta, K.; Oishi, S.; Teshima, K. *Cryst. Growth Des.* **2015**, *15*, 124−128.

(31) Cheng, L. K.; Bierlein, J. D.; Ballman, A. A. *J. Cryst. Growth* **1991**, *110*, 697−703.

(32) Akdogan, E. K.; Brennan, R. E.; Allahverdi, M.; Safari, A. *J. Electroceram.* **2006**, *16*, 159−165.

(33) Teshima, K.; Inagaki, H.; Tanaka, S.; Yubuta, K.; Hozumi, M.; Kohama, K.; Shishido, T.; Oishi, S. *Cryst. Growth Des.* **2011**, *11*, 4401−4405.

(34) Wang, F.; Wang, X. *Nanoscale* **2014**, *6*, 6398−6414.

DOI: 10.1021/ic502862t
Inorg. Chem. 2015, 54, 3237−3244

(35) Afanasiev, P. *Chem. Mater.* **1999**, *11*, 1999−2007.
(36) Afanasiev, P. *J. Phys. Chem. C* **2012**, *116*, 2371−2381.
(37) Afanasiev, P.; Aouine, M.; Deranlot, C.; Epicier, T. *Chem. Mater.* **2010**, *22*, 5411−5419.
(38) Burton, W. K.; Cabrera, N.; Frank, F. C. *Philos. Trans. R. Soc. London A* **1951**, *243*, 299−358.
(39) Matsushita, Y.; Ueda, H.; Ueda, Y. *Nat. Mater.* **2005**, *4*, 845−850.
(40) Qiu, X.; Miyauchi, M.; Yu, H.; Irie, H.; Hashimoto, K. *J. Am. Chem. Soc.* **2010**, *132*, 15259−15267.
(41) Macquart, R. B.; Gemmill, W. R.; Davis, M. J.; Smith, M. D.; zur Loye, H. C. *Inorg. Chem.* **2006**, *45*, 4391−4395.
(42) Ebbinghaus, S. G.; Aguiar, R.; Weidenkaff, A.; Gsell, S.; Reller, A. *Solid State Sci.* **2008**, *10*, 709−716.
(43) Gomathi Devi, L.; Narasimha Murthy, B. *Catal. Lett.* **2008**, *125*, 320−330.
(44) Kawashima, K.; Hojamberdiev, M.; Wagata, H.; Yubuta, K.; Oishi, S.; Teshima, K. *Cryst. Growth Des.* **2014**, *15*, 333−339.

DOI: 10.1021/ic502862t
Inorg. Chem. 2015, 54, 3237−3244